NANO LETTERS

2007
Vol. 7, No. 4
1105−1109

Effects of a Shell on the Electronic Properties of Nanowire Superlattices

Y. M. Niquet†

Département de Recherche Fondamentale sur la Matière Condensée, SP2M/L_Sim, CEA Grenoble, 38054 Grenoble Cedex 9, France

Received December 11, 2006; Revised Manuscript Received February 25, 2007

ABSTRACT

We compute the structural and electronic properties of core–shell InAs/GaAs nanowire superlattices using Keating's valence force field and a $sp^3d^5s^*$ tight-binding model. We show that the GaAs shell limits strain relaxation but homogenizes the hydrostatic strain distribution in the InAs layers. This prevents the formation of a strain-induced well in the conduction band at the surface of the nanowires, which was shown to trap the electrons in thin InAs layers (*Phys. Rev. B* 2006, *74*, 155304). The shell, however, enhances the piezoelectric field, which increases the separation between the electrons and holes in thick InAs layers. These results emphasize the intricate links between the structural and electronic properties of strained nanowire heterostructures.

1. Introduction. Catalytic growth techniques[1] have allowed the synthesis of semiconductor nanowire heterostructures with outstanding properties. The composition of the nanowires can actually be modulated along the growth axis[2−4] (axial structures) and/or radially[5−7] (core−shell structures). Axial nanowire heterostructures are very attractive because they can accommodate much larger misfit strains than conventional, quantum well heterostructures. Indeed, the critical thickness t_c is expected to increase with decreasing wire diameter[8] thanks to the enhancement of elastic strain relaxation by the free surfaces of the nanowires. Arbitrary heterostructures might even be grown below a (misfit-dependent) diameter where t_c eventually becomes infinite.[8] This opens up new opportunities for nanoscale devices: resonant tunneling diodes,[9] single-electron transistors,[10] and single-electron memories,[11] for example, have been successfully realized with InAs/InP nanowire heterostructures.

The effects of the residual strains on the electronic and optical properties of nanowire heterostructures have been, however, largely overlooked up to now. In ref 12, we have discussed the case of ⟨111⟩-oriented InAs/GaAs nanowire superlattices[13,14] (NWSLs) as a paradigm of large misfit strains. We have shown that strain relaxation is indeed efficient, but very inhomogeneous in thin InAs layers. It digs a well in the conduction band at the surface of the nanowires that traps the electrons.[15,16] We have also evidenced that the piezoelectric field could be large enough to separate the electrons from the holes in thick InAs layers, which strongly reduces the oscillator strength.

In this paper, we compute the effects of a GaAs shell on the structural and electronic properties of InAs/GaAs NWSLs using a $sp^3d^5s^*$ tight-binding model. We show that the shell limits strain relaxation in the InAs layers, but homogenizes the hydrostatic strain distribution. This prevents the formation of the above-mentioned strain-induced surface well in the conduction band. As a consequence, the electron wave functions are much less diffuse. The shell, however, strengthens the piezoelectric field, which increases the separation of the electron and hole in thick InAs layers. This suggests that the role played by the shell in the enhancement of the optical properties of the nanowires is more complex than anticipated. Beyond the case of InAs/GaAs NWSLs, these results emphasize the importance of strains and piezoelectric fields in the design of core and core−shell nanowire heterostructures.

In Section 2, we introduce the models used to compute the structural and electronic properties of the nanowire superlattices. We then discuss the properties of core−shell InAs/GaAs NWSLs in Section 3.

2. Theory. In this section, we discuss the geometry of the nanowires and the methods used to compute their structural and electronic properties. The most relevant physics (strains, piezoelectric fields, and image charge effects) has been included in an atomistic, $sp^3d^5s^*$ tight-binding model to achieve a realistic description of their electronic structure. Details can be found in ref 12.

The cores of the nanowires are [111]-oriented InAs/GaAs superlattices with the zinc-blende structure and radius $R_c = 10$ nm. The thickness of the InAs layers is $4 \leq t \leq 16$ nm, while the period of the superlattices is $L \simeq 40$ nm. The cores can be embedded in a GaAs shell with outer radius R_s. The dangling bonds at the surface of the nanowires are saturated with hydrogen atoms. In the following, we let $x = [1\bar{1}0]$, $y = [11\bar{2}]$, and $z = [111]$.

† E-mail: yniquet@cea.fr.

10.1021/nl0629097 CCC: $37.00
Published on Web 03/27/2007

The lattice mismatch between InAs and GaAs is $\epsilon_{||} = -6.69\%$. The relaxed atomic positions and actual period L of the superlattice are computed using Keating's valence force field (VFF) model.[17] The VFF elastic energy depends on the nearest-neighbor bond lengths and bond angles through "bond stretching" and "bond bending" constants. The latter are fitted to the bulk modulus and Poisson ratio ν_{111} of the materials.[18]

Strains displace the anions with respect to the cations, which gives rise to a piezoelectric polarization and potential. The piezoelectric polarization is, to first order, proportional to the shear strains in the cubic axis set. The importance of higher-order contributions has, however, been emphasized recently by Bester et al.[19] We have therefore improved over ref 12 by including second-order corrections in the calculation. Their effect will be discussed in Section 3B.

The one-particle electronic structure of the nanowires must be corrected for image charge effects. An electron added to the NWSL indeed repels nearby valence electrons onto the surface.[20,21] The interaction between the electron and these (negative) surface image charges decreases the affinity and rises the conduction band states. Conversely, the repulsion between a hole and its (positive) image charges increases the ionization energy and lowers the valence band states. The image charges (also known as self-energy) corrections, therefore, result in a substantial opening of the one-particle band gap of the nanowires. We have discussed the underlying physics and theory in ref 20. In a semiclassical approach, the effect of the image charges can be modeled by a local potential $\sum(r)$, which repels the electrons and holes from the surface, thus enhancing lateral confinement.

The one-particle states of the nanowires are computed with a first nearest-neighbor, two-center orthogonal $sp^3d^5s^*$ tight-binding (TB) model[21,22] based on the parametrization of Jancu et al.[23] We have added a strain-dependent, on-site coupling matrix between the p and the d orbitals to reproduce the valence band deformation potentials b and d.[12] We look for a few eigenpairs around the band gap using a Jacobi−Davidson algorithm as discussed in ref 20.

The exciton wave function is finally written as an uncorrelated electron−hole pair $\psi(\vec{\mathbf{r}}_e,\vec{\mathbf{r}}_h) = \psi_e(\vec{\mathbf{r}}_e)\psi_h(\vec{\mathbf{r}}_h)$. The electron wave function ψ_e is optimized in the electrostatic potential created by the hole (and likewise for the hole wave function ψ_h). Poisson's equation is solved with a finite-difference method.

3. Results. In this section, we discuss the strain distribution, piezoelectric field, and electronic properties of the nanowire superlattices (NWSLs) as a function of the shell radius R_s.

A. Strain Relaxation. The hydrostatic strain in a core−shell ($R_s = 12$ nm) NWSL with 4 nm thick InAs layers is plotted in Figure 1. $\delta\Omega/\Omega = \epsilon_{xx} + \epsilon_{yy} + \epsilon_{zz}$ is the local variation of the volume of the unit cell with respect to the unstrained materials. It would be as large as $\delta\Omega/\Omega = -9.56\%$ in a (hypothetic) InAs quantum well lattice-matched to GaAs (biaxial strain $\epsilon_{xx} = \epsilon_{yy} = -6.69\%$, $\epsilon_{zz} = 3.81\%$). The strain distribution in core-only nanowires with the same R_c has been discussed in detail in ref 12. The InAs layers

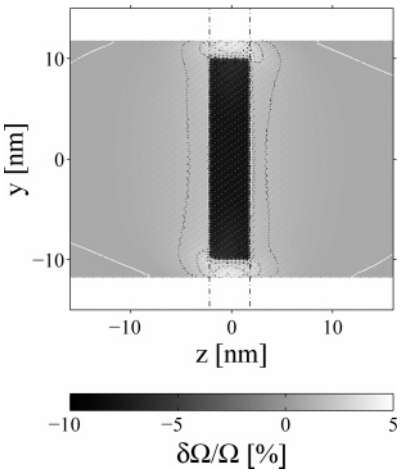

Figure 1. Hydrostatic strain $\delta\Omega/\Omega$ in a core−shell NWSL ($R_s = 12$ nm, $t = 4$ nm). The dots are the In/Ga atoms in the (yz) plane of the plot. The vertical, dash−dotted lines delimit the InAs layer. The spacing between isolevel curves is 1%, the white one being $\delta\Omega/\Omega = 0$.

expand outward by bending the surface of the nanowire and by transferring tensile strains to GaAs. The strain relaxation is efficient, although very inhomogeneous when $t \ll R$. Indeed, the center of thin InAs layers remains significantly compressed, while their periphery is overrelaxed ($\delta\Omega/\Omega > 0$).

The epitaxial growth of a GaAs shell around the nanowire puts back strains in the InAs layers. The shell indeed stiffens the surface and limits lateral strain relaxation. It also reduces the expansion of the InAs layers along z. The increase of strains within the InAs layers is evidenced in Figure 2a. The latter represents the relative variation $\Delta V/V$ of the volume of a 4 nm thick InAs layer (the average $\delta\Omega/\Omega$) as a function of R_s. While the core-only NWSL is significantly relaxed, $\Delta V/V$ tends to $\simeq -10\%$ when $R_s \rightarrow \infty$, slightly below the biaxial reference discussed above. The increase is sizable even for small R_s because the number of atoms per unit of length in the core and in the shell become rapidly comparable. The shell also affects the relaxation of thick InAs layers, as shown in Figure 2b. The 16 nm thick InAs layers are indeed almost completely relaxed in the core-only NWSL, while they are hardly more relaxed than the 4 nm thick layers when $R_s = 12$ nm.

The growth of a shell homogenizes the hydrostatic strain distribution in the InAs layers, as shown by the comparison of Figure 1 (this paper) with Figure 2 of ref 12. This is also evidenced in the inset of Figure 2a, which represents the rms variation $\sigma_{\delta\Omega/\Omega} = [\langle(\delta\Omega/\Omega)^2\rangle - (\Delta V/V)^2]^{1/2}$ of the hydrostatic strain in 4 nm thick InAs layers ($\langle ... \rangle$ is a spatial average over these layers). The effects of the strain distribution on the electronic properties of the nanowires will be discussed in Section 3C.

Thin shells sustain large strains. They are strongly dilated along the growth axis [$\epsilon_{zz} \simeq 5\%$ for $t = 4$ and $R_s = 12$ nm] and sheared in the (xy) plane [ϵ_{xy} and $(\epsilon_{xx} - \epsilon_{yy})/2$ up to $\simeq 3.5\%$]. Part of these strains are transferred from the shell to the core when increasing R_s. This questions the structural quality of the shell around the InAs layers. On one hand,

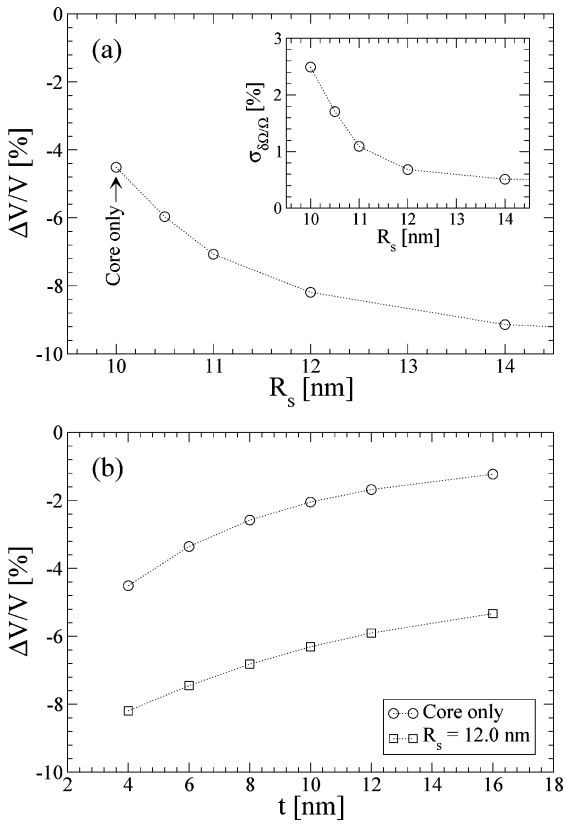

Figure 2. (a) Average hydrostatic strain $\Delta V/V$ in 4 nm thick InAs layers as a function of R_s. The inset represents the rms variation $\sigma_{dW/\Omega}$ of the hydrostatic strain in these InAs layers. (b) $\Delta V/V$ as a function of t in core-only and core−shell nanowires ($R_s = 12$ nm).

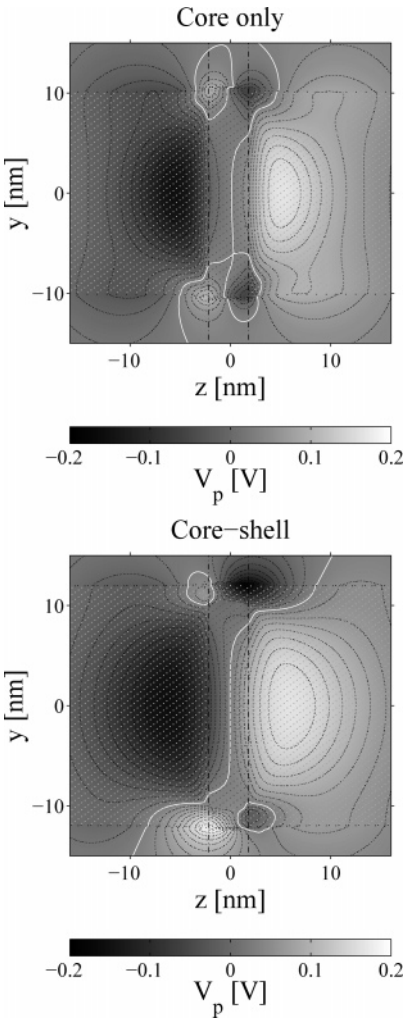

Figure 3. Piezoelectric potential V_p in a core-only and core−shell NWSL ($R_s = 12$ nm, $t = 4$ nm). The spacing between isolevel curves is 20 mV, the white one being $V_p = 0$.

ref 6 for example shows that the growth of a mismatched shell is actually possible. On the other hand, the shell might be defective, which would limit the pressure onto the core. While this issue can only be settled experimentally, the conditions for the onset of plastic strain relaxation in the shell will ultimately depend on t and R_c. We will therefore now focus on the 4 nm thick InAs layers, whose dimensions are comparable with those of (embedded) Stransky−Krastanov quantum dots.

B. Piezoelectric Potential. The piezoelectric potential $V_p(\vec{\mathbf{r}})$ in a core-only and a core−shell ($R_s = 12$ nm) NWSL with 4 nm thick InAs layers is plotted in Figure 3 (including second-order corrections[19]). As discussed in ref 12, the piezoelectric polarization density $\vec{\mathbf{P}}(\vec{\mathbf{r}})$ can be replaced with an equivalent distribution of bound charges $\rho_p(\vec{r}) = -\nabla\vec{\mathbf{P}}(\vec{\mathbf{r}})$. Because $\vec{\mathbf{P}}(\vec{\mathbf{r}})$ is mostly aligned with the growth axis, its main effects are to transfer bound charges (i) from one interface to the other through the InAs layer and (ii) from the GaAs barriers to the nearest interface. This leaves two long-range tails of charges in GaAs, which are clearly visible on Figure 3. There are, in addition, complex transfers of charges between the inner and outer surfaces of the shell in core−shell systems.

The second-order piezoelectric corrections tend to enhance the polarization under tensile strain and to revert its sign under compressive strain. In the core-only NWSL, $P_z = \vec{\mathbf{P}}\cdot\vec{\mathbf{z}}$ is actually negative at the surface of the InAs layer (like in ref 12), but positive around its axis. As a consequence, the sign of $E_z = -\partial V_p/\partial z$ also changes between the axis and the surface (see Figure 3). The piezoelectric field at the center of the InAs layer is (incidentally) of the same order of magnitude as but opposite to ref 12. The situation however becomes qualitatively similar to that of ref 12 at larger t as strain relaxation gains the whole layer. Indeed, the piezoelectric field is not reversed any more beyond $t \simeq 6$ nm.

The piezoelectric field is (like the strains) larger and more uniform in core−shell than in core-only nanowires. The difference of potential along the axis of the InAs layer indeed lies in the $\lesssim$300 meV range in core−shell NWSLs ($R_s = 12$ nm, $4 \le t \le 16$ nm), while it lies in the $\lesssim$100 meV range in core-only NWSLs. The piezoelectric field at the center of the InAs layer is also reversed in core−shell nanowires below $t \simeq 6$ nm.

C. Electronic Structure. The lowest-lying electron (E1) and hole (H1) wave functions in a core-only and a core−shell ($R_s = 12$ nm) NWSL with 4 nm thick InAs layers are plotted in Figures 4 and 5. Their energies (with respect to the valence band edge of bulk InAs) are reported in Table 1.

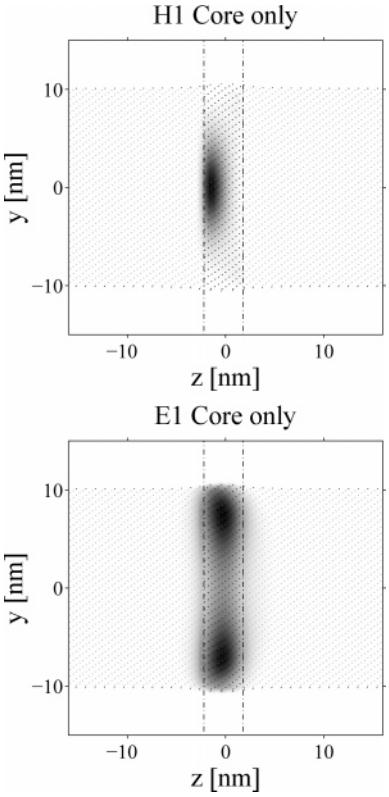

Figure 4. Square of the highest hole (H1) and lowest electron (E1) wave functions in a core-only NWSL ($t = 4$ nm).

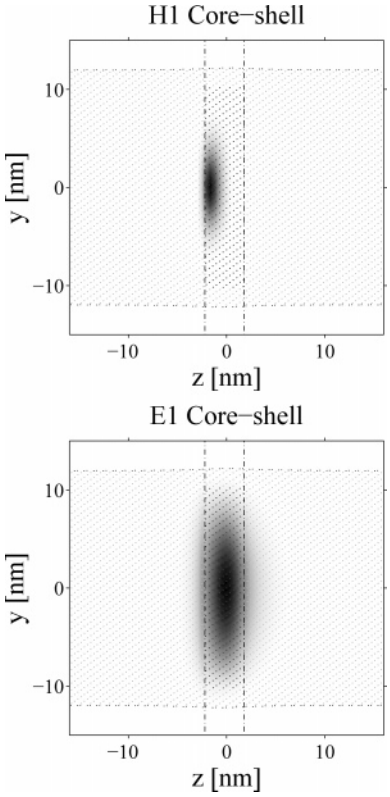

Figure 5. Square of the highest-hole (H1) and lowest-electron (E1) wave functions in a core−shell NWSL ($R_s = 12$ nm, $t = 4$ nm).

Table 1. Energy (E), Strain-Induced Shift (Δ_s), Expectation Value of the Piezoelectric Potential ($\langle V_p \rangle$), and Image Charge Correction ($\langle \Sigma \rangle$) as a Function of the Radius R_s of the Shell for the Lowest-Lying Hole (H1) and Electron (E1) States ($t = 4$ nm)

R_s (nm)		E (eV)	Δ_s (meV)	$\langle V_p \rangle$ (meV)	$\langle \Sigma \rangle$ (meV)
core	H1	−0.007	48.4	16.3	−38.4
	E1	0.952	143.5	4.3	50.6
11.0	H1	0.027	53.7	40.2	−31.6
	E1	1.039	238.9	9.8	36.4
12.0	H1	0.046	60.3	52.1	−28.6
	E1	1.071	276.6	2.3	30.7

As discussed in ref 12, strain relaxation has a strong impact on the electronic properties of the nanowires. In particular, the hydrostatic strain shifts the conduction band energy by $\Delta E_c \simeq a_c \delta\Omega/\Omega$, where $a_c = -5.12$ eV in the present TB model. The inhomogeneous strain distribution in core-only NWSLs, therefore, digs a well in the conduction band at the (overrelaxed) surface of the nanowires. This well traps the electrons in the 4 nm thick InAs layers, which likely increases the probability of capture by nearby surface defects. The growth of a shell naturally moves these defects away. It also smooths the well out as the hydrostatic strain distribution becomes more and more homogeneous. The electrons actually appear well confined inside the InAs layer as soon as $R_s \gtrsim 11$ nm. The hole wave function does not look, on the other hand, much affected by the shell. It is always squeezed against one of the interfaces by the piezoelectric field. The hole, however, moves from one side of the layer to the other around $t = 6$ nm (reversal of the piezoelectric field). The piezoelectric field further separates the electron from the hole in thicker layers (in core-only and more so in core−shell nanowires), which steadily degrades the optical properties.[12]

The strain-induced energy shifts Δ_s, the expectation values of the piezoelectric potential ($\langle V_p \rangle$), and the image charge corrections ($\langle \Sigma \rangle$) in the core-only and core−shell NWSLs ($t = 4$ nm) are given in Table 1. The second-order corrections to the piezoelectric polarization do not have much effect on these figures (see ref 12 for a comparison with first-order data) because they mostly result (in that particular case) in a reversal of the piezoelectric field at the center of the InAs layer. The larger and more homogeneous strains in the core−shell systems (no surface well) raise the E1 energy up to 120 meV above the core-only NWSL. The H1 energy is, on the other hand, slightly shifted upward by the stronger piezoelectric field and by the decrease of the image charge correction with increasing R_s.[12] The one-particle gap is thus 66 meV larger for $R_s = 12$ nm than in the core-only nanowire. The excitonic correction lowers the optical band gap by $E_X = 88$, 84, and 80 meV, respectively, in the core-only and core−shell systems with $R_s = 11$ and $R_s = 12$ nm. The slow decrease of E_X with increasing R_s can again be traced back to the decrease of the image charge contributions to the exciton energy (interaction of the electron with the image charges of the hole and vice-versa).[12]

4. Conclusion. We have computed the structural and electronic properties of ⟨111⟩-oriented core−shell InAs/GaAs nanowire superlattices. We show that the shell limits strain relaxation in the InAs layers, but homogenizes the hydrostatic

strain distribution. This prevents the formation of a strain-induced well in the conduction band at the surface of the nanowires, which was shown to trap the electrons in core-only systems. The growth of a shell, however, enhances the piezoelectric field, which increases the separation of the electron and hole in thick InAs layers. From the experimental point of view, the optical spectroscopy of InAs/GaAs NWSLs has not been very successful up to now.[13,14] Switching the cation (In/Ga), which alloys with the catalyst,[24] actually appears to be more difficult than switching the anion. The advent of catalyst-free techniques[25] might, however, revive the interest in InAs/GaAs heterostructures. Moreover, the above conclusions likely apply to many other materials. Indeed, while the lattice mismatch is large in InAs/GaAs, the effective mass of the electrons ($m^* = 0.023m_0$) and the piezoelectric constants of InAs are quite small. The electrons and holes might, therefore, be trapped by the strains in other heterostructures with much lower lattice mismatches. The design of nanowire heterostructures should, therefore, deal with the effects of strains and piezoelectric fields, taking advantage of the shell to tune the properties of the wires.

Acknowledgment. This work was supported by the French "Action Concertée Incitative" (ACI) "TransNanofils" and by the European Integrated Project (IP) NODE (EU contract no. 015783 NODE).

References

(1) Morales, A. M.; Lieber, C. M. *Science* **1998**, *279*, 208−211.
(2) Wu, Y.; Fan, R.; Yang, P. *Nano Lett.* **2002**, *2*, 83−86.
(3) Gudiksen, M. S.; Lauhon, L. J.; Wang, J.; Smith, D. C.; Lieber, C. M. *Nature* **2002**, *415*, 617−620.
(4) Björk, M. T.; Ohlsson, B. J.; Sass, T.; Persson, A. I.; Thelander, C.; Magnusson, M. H.; Deppert, K.; Wallenberg, L. R.; Samuelson, L. *Nano Lett.* **2002**, *2*, 87−89.
(5) Lauhon, L. J.; Gudiksen, M. S.; Wang, D.; Lieber, C. M. *Nature* **2002**, *420*, 57−61.
(6) Lu, W.; Xiang, J.; Timko, B. P.; Wu, Y.; Lieber, C. M. *Proc. Natl. Acad. Sci. U.S.A.* **2005**, *102*, 10046−10051.
(7) Qian, F.; Gradečak, S.; Li, Y.; Wen, C.-Y.; Lieber, C. M. *Nano Lett.* **2005**, *5*, 2287−2291.
(8) Glas, F. *Phys. Rev. B* **2006**, *74*, 121302.
(9) Björk, M. T.; Ohlsson, B. J.; Thelander, C.; Persson, A. I.; Deppert, K.; Wallenberg, L. R.; Samuelson, L. *Appl. Phys. Lett.* **2002**, *81*, 4458−4460.
(10) Thelander, C.; Martenson, T.; Björk, M. T.; Ohlsson, B. J.; Larsson, M. W.; Wallenberg, L. R.; Samuelson, L. *Appl. Phys. Lett.* **2003**, *83*, 2052−2054.
(11) Thelander, C.; Nilsson, H. A.; Jensen, L. E.; Samuelson, L. *Nano Lett.* **2005**, *5*, 635−638.
(12) Niquet, Y. M. *Phys. Rev. B* **2006**, *74*, 155304.
(13) Ohlsson, B. J.; Björk, M. T.; Persson, A. I.; Thelander, C.; Wallenberg, L. R.; Magnusson, M. H.; Deppert, K.; Samuelson, L. *Physica E* **2002**, *13*, 1126−1130.
(14) Panev, N.; Persson, A. I.; Sköld, N.; Samuelson, L. *Appl. Phys. Lett.* **2003**, *83*, 2238−2240.
(15) Straub, H.; Brunthaler, G.; Faschinger, W.; Bauer, G.; Vieu, C. *J. Cryst. Growth* **1996**, *159*, 451−454.
(16) Niquet, Y. M.; Priester, C.; Mariette, H. *Phys. Rev. B* **1997**, *55*, R7387−7390.
(17) Keating, P. N. *Phys. Rev.* **1966**, *145*, 637−645.
(18) *Physics of Group IV Elements and III−V Compounds*; Landolt−Bornstein New Series, Group III, Vol. 17a; Madelung, O., Schulz, M., Weiss, H., Eds.; Springer-Verlag: New York, 1982.
(19) Bester, G.; Wu, X.; Vanderbilt, D.; Zunger, A. *Phys. Rev. Lett.* **2006**, *96*, 187602.
(20) Niquet, Y. M.; Lherbier, A.; Quang, N. H.; Fernández-Serra, M. V.; Blase, X.; Delerue, C. *Phys. Rev. B* **2006**, *73*, 165319.
(21) Delerue, C.; Lannoo, M. *Nanostructures: Theory and Modelling*; Springer: New York, 2004.
(22) Slater, J. C.; Koster, G. F. *Phys. Rev.* **1954**, *94*, 1498−1524.
(23) Jancu, J.-M.; Scholz, R.; Beltram, F.; Bassani, F. *Phys. Rev. B* **1998**, *57*, 6493−6507.
(24) Persson, I. A.; Larsson, M. W.; Stenstrom, S.; Ohlsson, B. J.; Samuelson, L.; Wallenberg, L. R. *Nat. Mater.* **2004**, *3*, 677−681.
(25) Noborisaka, J.; Motohisa, J.; Fukui, T. *Appl. Phys. Lett.* **2005**, *86*, 213102.

NL0629097